ORIGINAL PAPER

CrossMark

Estimating engineering properties of igneous rocks using semi-automatic petrographic analysis

Saeed Aligholi[1,2] · Gholam Reza Lashkaripour[1] · Mohammad Ghafoori[1]

Abstract

An experimental study that contributes to the understanding of the relationships between petrographic features and engineering properties of igneous rocks is conducted. To this end, a wide range of igneous rocks were tested for their engineering properties including abrasivity (Cerchar abrasivity index), mechanical (point load strength index $Is_{(50)}$), basic physical (dry density and porosity) and dynamic (P-wave velocity) characteristics. Moreover, a semi-automatic method has been developed to analyze petrographic data that relies on digital image acquisition from representative parts of representative thin sections of samples, semi-automatic image segmentation and image analysis. The method quantifies 18 petrographic features including size descriptors (area, perimeter, equivalent circular diameter, minimum Feret's diameter, maximum Feret's diameter), shape descriptors (elongation, orientation, eccentricity, compactness, rectangularity, solidity, convexity), rock fabric coefficients (index of interlocking, index of grain size homogeneity, texture coefficient) and mineralogical indices (saturation index, feldspathic index, colouration index). The Pearson's correlation coefficient and multivariate regression analysis are employed to analyze the relationships between extracted petrographic features and engineering properties. In general, fine-grained and basic igneous rocks compared to the acidic and coarse-grained ones possess higher engineering quality and lower abrasiveness potential. The results imply that mineralogical composition tends to be more important than rock fabric characteristics in determining the engineering properties of igneous rocks. Furthermore, among rock fabric characteristics, size descriptors have significant influence on the engineering properties. Overall, it was found that mineralogical composition and rock fabric characteristics provide a suitable complement to reliably predict engineering properties of igneous rocks.

Introduction

It is believed that engineering properties of intact rocks are some functions of their petrographic features and physical characteristics. Rocks are mostly composed of varying percentages of minerals with different grain size, grain shape and micro-fabric characteristics (Aligholi et al. 2017a). Many research studies have dealt with the relationship between rock fabric and mechanical properties of different rock types (Olsson 1974; Hugman and Friedman 1979; Howarth and Rowlands 1987; Hatzor and Palchik 1997; Akesson et al. 2003; Jeng et al. 2004; Přikryl 2001, 2006; Ozturk and Nasuf 2013; Tandon and Gupta 2013; Pappalardo et al. 2016). Rock fabric properties affecting the mechanical performance of rocks are grain size, shape and degree of interlocking, porosity (crack and pore), grain orientation and the nature of grain boundaries (Howarth and Rowlands 1987). On the other hand, some research studies were performed to investigate the relationship between mineral constituents and mechanical behavior of different rocks (Bell 1978; Fahy and Guccione 1979; Gunsallus and Kulhawy 1984; Ulusay et al. 1994; Tugrul and Zarif 1999; Zorlu et al. 2008; Yilmaz et al. 2011; Hashemnejad et al. 2016; Moradizadeh et al. 2016). As noted by Howarth and Rowlands (1987), as well as Tandon and Gupta (2013), some of these studies reported contradict outcomes, for example about the relationship between quartz

✉ Gholam Reza Lashkaripour
lashkaripour@um.ac.ir

[1] Department of Geology, Faculty of Science, Ferdowsi University of Mashhad, Mashhad, Iran

[2] Department of Civil Engineering, Monash University, Clayton, VIC 3800, Australia

content and UCS in sandstone. This may be due to different types of structural and non-structural conditions. Structural conditions are pertaining to both the genesis of the rocks and the environmental conditions such as regional tectonic setups, temperature and hydrothermal solution, which cause different degrees of alteration and weathering, while the non-structural ones are mostly related to measurement methodology and equipment conditions.

There are diverse studies presenting the qualitative relationship between rock fabric and mechanical properties of rocks, but quantitative approach of petrographic characterization is adopted in rock mechanics studies only recently (Brosch et al. 2000; Raisanen 2004; Přikryl 2001, 2006; Gupta and Sharma 2012; Ozturk and Nasuf 2013; Tandon and Gupta 2013). This is probably due to laborious and time consuming factors (Přikryl 2006; Gupta and Sharma 2012). The need for the rapid and accurate quantitative processing of microstructures has increased during recent decades and leads to the implementation of computer assisted image analysis in material sciences including geology (Přikryl 2006). Combining thin section examination with computer programs that analyze rock photomicrograph allow fast measurement and quantitative analysis of thin section features (Reedy 2006).

In this study we dealt with the problem of automated rock photomicrograph analysis, as well as the effects of petrographic characteristic including rock fabric features and mineralogical composition on engineering properties of igneous rocks. For such purpose with the aid of digital microscopy and image processing techniques, first representative digital images from representative thin sections of studied igneous rocks were segmented, then rock fabric features and mineralogical indices were extracted and correlated with selected engineering properties.

Materials

The aim of this research is to inquire the relationships between petrographic features and engineering properties of igneous rocks; for this purpose, 28 various types of igneous rocks have been sampled in 15 different locations of Iran (Fig. 1). A wide range of igneous rocks including plutonic, hypabyssal and extrusive are examined in this study (Table 1). According to Anon (1995), all samples were unweathered or slightly weathered, and blocky samples carefully checked to ensure they were homogeneous and free from visible plans of weakness. Each block sample was drilled or cut to obtain cylindrical cores or blocky specimens to inspect engineering properties.

Fig. 1 Location map of the rock samples

Table 1 Modal analysis and rock names of the studied rocks

Rock code	Qtz (%)	Pl (%)	Afs (%)	Bt (%)	Ms (%)	Am (%)	Chl (%)	Cpx (%)	Opx (%)	Ol (%)	Grt (%)	OM (%)	Ep (%)	Gl (%)	AM <1%	Rock name*
R1	28	35	20	17	–	–	–	–	–	–	–	–	–	–	Zrn	Micro-monzogranite
R2	38	24	28	3	7	–	–	–	–	–	–	–	–	–	–	Monzogranite
R3	31	21	34	4	9	–	1	–	–	–	–	–	–	–	–	Monzogranite
R4	–	41	–	–	–	5	–	8	5	–	2	2	1	36	–	Hyalo-basaltic andesite
R5	32	34	27	4	–	2	–	–	–	–	–	1	–	–	–	Monzogranite
R6	–	47	–	–	–	4	–	19	5	9	–	13	3	–	–	Basalt
R7	37	22	31	7	–	1	2	–	–	–	–	–	–	–	Zrn	Monzogranite
R8	37	18	38	5	–	1	1	–	–	–	–	–	–	–	Zrn	Syenogranite
R9	41	14	40	2	–	1	2	–	–	–	–	–	–	–	Zrn	Syenogranite
R10	26	17	48	6	–	–	1	–	–	–	–	–	2	–	–	Syenogranite
R11	12	34	7	9	–	3	–	–	–	–	–	3	–	32	–	Hyalo-dacite
R12	29	38	22	4	–	3	2	–	–	–	1	1	–	–	–	Monzogranite
R13	14	46	16	–	–	12	9	–	–	–	–	3	–	–	Zrn	Quartz Monzodiorite
R14	12	59	3	–	–	7	9	4	–	–	–	6	–	–	–	Andesite
R15	1	64	1	3	–	23	3	–	–	–	1	4	–	–	Spn	Diorite
R16	4	63	6	–	–	14	8	–	–	–	–	5	–	–	–	Andesite
R17	28	29	35	5	–	–	3	–	–	–	–	–	–	–	–	Monzogranite
R18	–	48	–	4	–	3	–	16	6	–	9	6	8	–	–	Gabbro
R19	–	36	–	5	–	7	–	18	11	14	–	2	7	–	–	Gabbro
R20	–	57	2	4	–	6	–	–	11	8	1	5	6	–	Zrn	Diorite
R21	–	58	3	4	–	4	–	13	3	7	1	4	3	–	–	Diorite
R22	13	33	41	1	–	9	–	–	–	–	–	3	–	–	–	Quartz Monzonite
R23	7	40	44	1	–	6	–	–	–	–	–	2	–	–	–	Quartz Monzonite
R24	12	24	56	2	–	4	–	–	–	–	–	2	–	–	–	Quartz Syenite
R25	3	69	7	4	–	14	–	–	–	–	–	3	–	–	–	Andesite
R26	27	41	19	6	–	4	1	–	–	–	–	2	–	–	Spn	Granodiorite
R27	29	45	9	7	–	6	2	–	–	–	1	1	–	–	Spn	Granodiorite
R28	–	59	–	8	–	5	–	12	4	–	–	2	6	4	–	Micro-gabbro

*According to optical microscopy studies (Streckeisen, 1976)

**Qtz: Quartz; Pl: Plagioclase; Afs: Alkali feldspar; Bt: Biotite; Ms.: Muscovite; Am: Amphibole; Chl: Chlorite; Cpx: Clino pyroxene; Opx: Orthopyroxene; Ol: Olivine; Grt: garnet; OM: Opac minerals; Ep: Epidote; Gl: glass; AM: Accessory minerals; Zrn: zircon; Spn: Sphene

Thin sections were also prepared from each rock sample for petrographic analysis.

Semi-automatic petrography

Image acquisition method

In this study, thin sections are imaged using a digital camera mounted on a petrographic microscope. The microscope is equipped with an analyzer and polarizer that might be rotated independently. All images were captured under cross-polarized light (XPL) using red, green and blue (RGB) components in JPG format with a resolution of 5184×3456 pixels, which are resized to 1037×692 to shorten the processing time.

Depending on grain size, the variations in grain size, and rock homogeneity, at least two thin sections were studied for each rock sample. Measurement of 50-200 grains is often needed in order to adequately characterize a single thin section (Middleton et al. 1985). Considering the grain size (i.e. mean equivalent circular diameter of grains), the studied igneous rocks were classified for image acquisition as follows:

- Fine-grained rocks (mean grain size 0.08 – 0.15 mm): With respect to homogeneity of these rocks, image/ images were taken from 1 to 5 parts of thin sections [i.e. center, upper (left and right) and lower (left and right) parts of a thin section] under 100× microscope magnification.
- Fine- to medium-grained rocks (mean grain size 0.15 – 0.30 mm): With respect to homogeneity of these rocks, image/images were taken from one to five parts of thin sections under 40× microscope magnification.
- Medium- to coarse-grained rocks (mean grain size 0.30 – 1 mm): With respect to homogeneity of these rocks, one or two horizontal line/lines were scanned along the thin sections under 40× or 25× microscope magnifications. For such purpose, firstly one or two representative scan line/ lines in a thin section selected [Fig. 2a], then imaging carried out as follows:
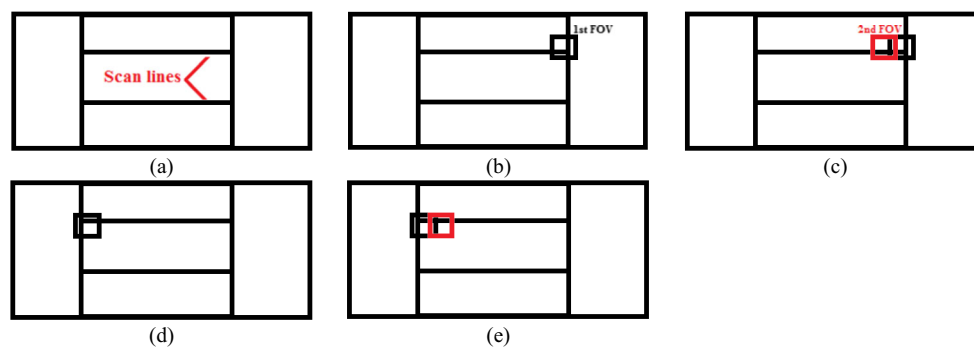
Fig. 2 Schematic view of image acquisition of medium to coarse grained rocks; (**a**) selected scan lines in thin section; (**b**) first FOV on the right end of the scan line, in which the selected scan line appears at the lower part of the FOV; (**c**) second FOV on the right end of the scan line, which has an overlap with first FOV; (**d**) first FOV on the left end of the scan line, in which the selected scan line appears at the upper part of the FOV; (**e**) second FOV on the left end of the scan line, which has an overlap with the former FOV

a) Camera field of view (FOV) was fixed at the end of a scan line where the scan line located at the lower part of camera FOV (Fig. 2b), and first image was taken.
b) Then, using a mechanical stage thin section moved towards another end of the scan line and second image was taken, it is notable that the first and the second images had about 30-40% overlap with each other (Fig. 2c). The scheme was continued to the other end of the scan line.
c) Next, the thin section was moved vertically where the scan line located at the upper part of camera FOV (Fig. 2d), and next image was taken.
d) After that, thin section was moved towards the point at which the imaging was started, and next image was taken. This image had about 30-40% overlap with the former image (Fig. 2e). The scheme was continued up to the point at which the imaging was started.

Finally, these image series were merged to each other to create a unified image for further analysis, as an example, Fig. 3 illustrates one of the unified images obtained from R26 sample.
• Coarse-grained rocks (mean grain size 1 – 1.3 mm): With respect to homogeneity of these rocks, two or more scan lines of thin sections were scanned under 25× microscope magnification which had side by side overlaps.

It is notable that grain size (mean equivalent circular diameter of grains) of the studied rocks ranged between 0.09 mm to 1.21 mm.

Image segmentation method

Quantitative analysis of micropetrographic data such as rock fabric and mineralogical composition is a time consuming task. Thus, (semi-)automatically quantifying grain siz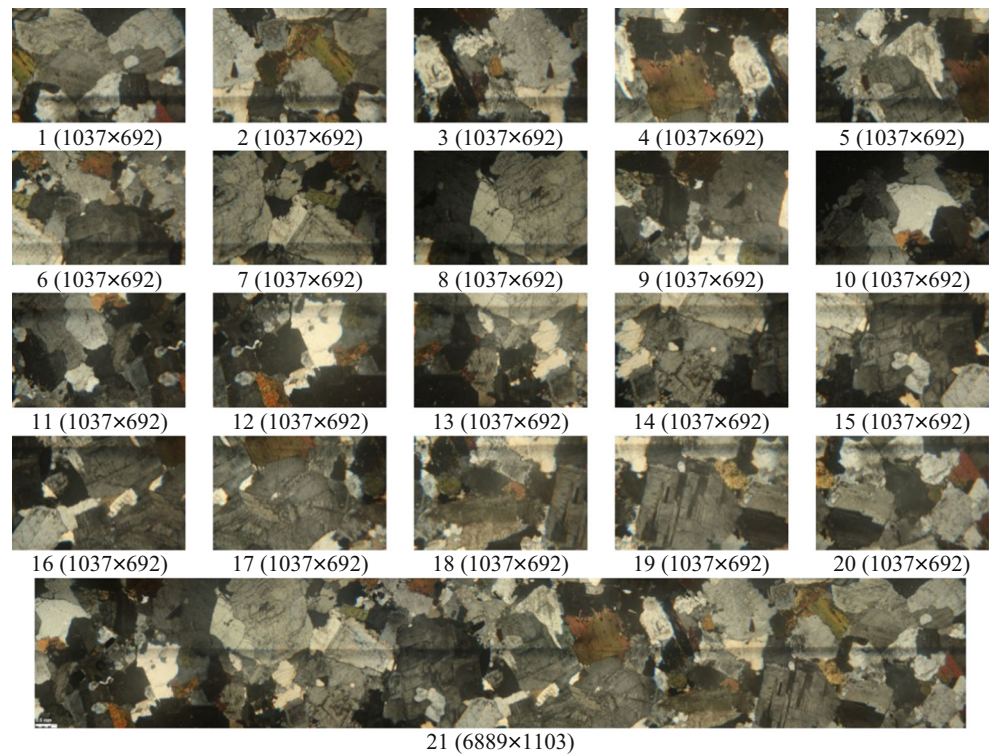e, grain shapes and grain contacts are commonly applied to characterize mineral shape fabrics and determine modal rock composition (Asmussen et al. 2015). The technique of (semi-)automatic rock photomicrograph segmentation as a prerequisite for any rock fabric analysis scheme is a challenging, popular, and important research topic in computational geology, mineralogy, and mining engineering (Izadi et al. 2015).

So far, several image processing and pattern recognition techniques such as color analysis, textural analysis, and frequency domain analysis are employed in rock analysis; most of such techniques are devoted to the field of (semi-)automatic rock photomicrograph segmentation (Goodchild and Fueten 1998; Heilbronner 2000; Zhou et al. 2004; Barraud 2006; Obara 2007; Fueten and Mason 2007; Filho et al. 2013), as well as mineral identification (Ross et al. 2001; Thompson et al. 2001; Marschallinger and Hofmann 2010; Aligholi et al. 2015, 2017b) as two prerequisite for any rock analysis scheme. A number of petrographic image segmentation techniques such as threshold, boundary-based, region-based, and hybrid techniques can be found in the previously mentioned literature. In this paper, a method has been developed to segmenting petrographic images, which relies on the following steps:

Step 1 (Convert RGB image to grayscale): 24-bit RGB images were transformed into eight-bit intensity images by forming a weighted sum of the R, G, and B components.

Step 2 (Image enhancement): This step involves two cycles of noise reduction by means of median filter, enhancing the contrast of images using histogram equalization, and opening-closing by reconstruction, which uses the fast hybrid grayscale reconstruction algorithm described in (Vincent 1993). Such morphological operations reduce negative effects of noise within grain regions (e.g. cracks, twinning and undulose extinction) whilst retaining the shape of the grains is of much interest.

Fig. 3 Prepared images from a thin section of the R26 sample with about 1 mm mean grain size under cross polarized light. (1-20) Camera FOV at different parts of the thin section, in which selected scan line appears at lower or upper of them (the scan line indicated with a pencil); (21) unified image from 1 to 20 images (size of each images indicated, the length of scan line is 29.13 mm, and the microscope magnification is 25×)

1 (1037×692) 2 (1037×692) 3 (1037×692) 4 (1037×692) 5 (1037×692)

6 (1037×692) 7 (1037×692) 8 (1037×692) 9 (1037×692) 10 (1037×692)

11 (1037×692) 12 (1037×692) 13 (1037×692) 14 (1037×692) 15 (1037×692)

16 (1037×692) 17 (1037×692) 18 (1037×692) 19 (1037×692) 20 (1037×692)

21 (6889×1103)

Step 3 (Image segmentation): To segment grains in rocks under examination an algorithm described by Jin (2012) was employed. The method has four main following steps:

- Computing a gradient map or intensity map from the image;
- Computing a cumulative distribution function from the gradient map;
- Modifying the map using the selected scale level value; and
- Segments the modified gradient map using a watershed transform.

The method has good segmentation results, if good preprocessing such as noise reduction and contrast enhancement (step 2), as well as adequate adjustment of dynamic parameters (i.e. scale level and edge level) are applied. The scale level is computed from a normalized cumulative distribution function of the pixel values in the image. For example, the lowest 20% of gradient magnitude values are discarded from the gradient image, if a scale level of 20 is employed. Increasing the scale level keeps objects with the most distinct edges. The method uses of edge level as a threshold for merge adjacent segments, increasing the merge level results in more merging. Over-segmented areas were merged using full lambda schedule which iteratively merges adjacent segments based on a combination of spectral and spatial information (Robinson et al. 2002). Sobel edge detection method is provided for

applying a watershed algorithm on the modified gradient map. The watershed transform is based on the concept of hydrologic watersheds (Vincent and Soille 1991).
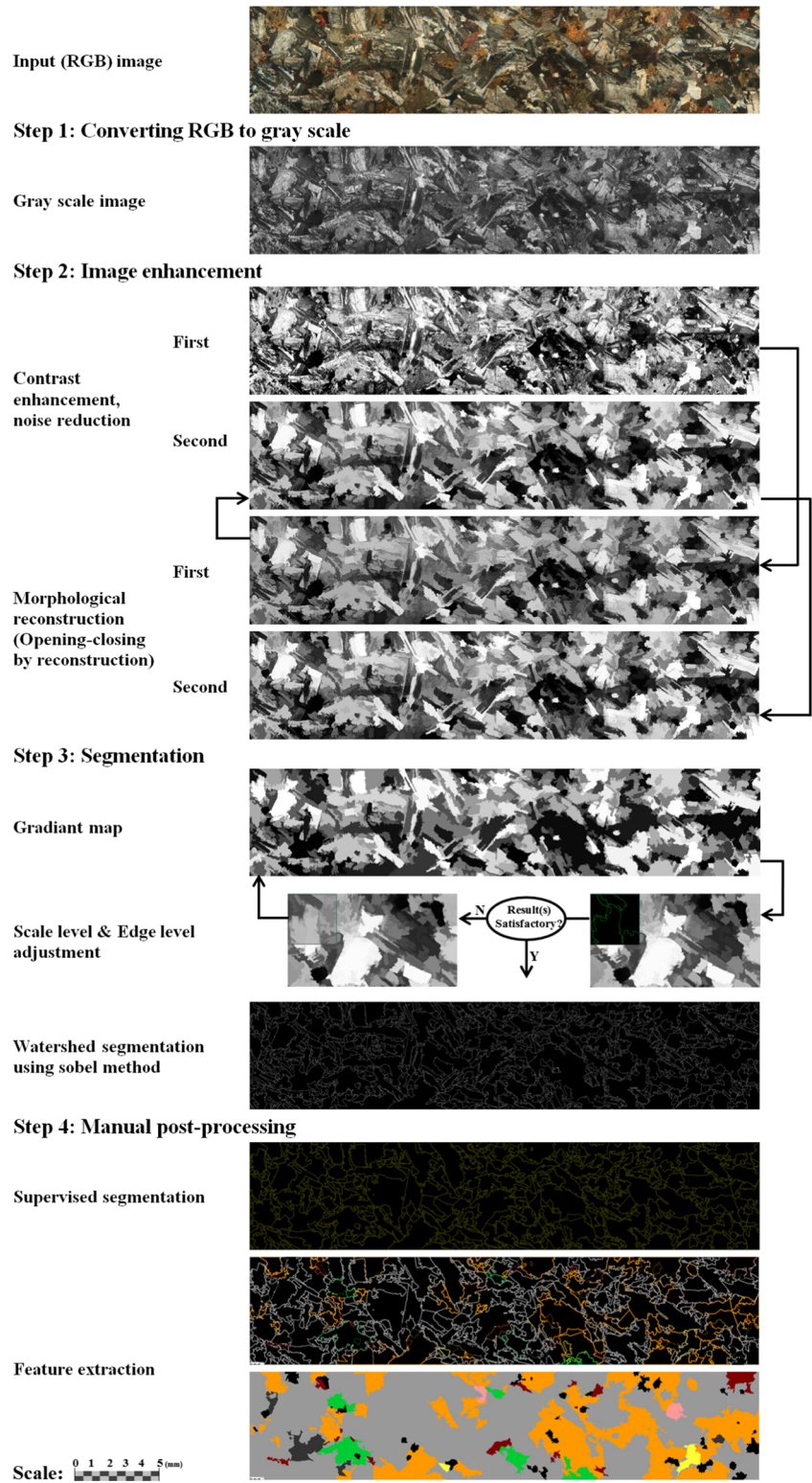
In this method, prior to segmenting the modified gradient map, a preview window of the digital image can be segmented at the selected scale level and merge level to determine if the selected parameters will give the desired segmentation. The dynamics parameters are the variables in this algorithm and are different for each of rocks under examination, based on our experience a scale level value about 70-80%, and an edge level value of about 80-90 give satisfactory segmentation results for enhanced gray scale petrographic images. It is notable that after segmentation, objects less than minimum grain size of each rock are removed. The detailed algorithm used in application of the described procedure is presented in Fig. 4.

Step 4 (Manual post-processing): Texture features of some minerals, for example plagioclase and microcline that show twinning commonly causes faulty segmentation of these minerals; so, a post-processing step is required.

Feature extraction and microstructural analysis

For the sake of petrographic features extraction, firstly segmented photomicrographs scaled using converted the pixel values to millimeters by a conversion factor, which is obtained

Fig. 4 Segmentation flow sheet
of unified photomicrograph from
a thin section of the R15 sample

Input (RGB) image

Step 1: Converting RGB to gray scale

Gray scale image

Step 2: Image enhancement

First

**Contrast
enhancement,
noise reduction**

Second

First

**Morphological
reconstruction
(Opening-closing
by reconstruction)**

Second

Step 3: Segmentation

Gradiant map

**Scale level & Edge level
adjustment**

Result(s)
Satisfactory?

N   Y

**Watershed segmentation
using sobel method**

Step 4: Manual post-processing

Supervised segmentation

Feature extraction

Scale: 0 1 2 3 4 5 (mm)

based on a standard scaled thin section for each microscope magnification. Then, the mean of basic size and shape descriptors described in Table 2 of all grains are obtained for each rock (Table 3). It is notable that for each rock, the mean of orientation of all grains subtracted from 90 and the absolute value of this number is reported as the orientation; higher

Table 2 Summary of the studied size and shape descriptors

Category	Parameter	Computation
Size descriptor	Area	Number of pixels in the object
	Perimeter	Length of the outline of the object
	Size	Equivalent circular diameter
	Minimum Feret's diameter	Minimum caliper
	Maximum Feret's diameter	Maximum caliper
Shape descriptor	Elongation	Ratio of the maximum to the minimum Feret's diameter
	Orientation	Angle between the horizontal axis and the major axis of the ellipse equivalent to the object (0-180 degrees, counterclockwise)
	Eccentricity	Ratio between the major and the minor axis of the ellipse equivalent to the object
	Compactness	Ratio of the area of the object to the area of a circle with the same perimeter
	Rectangularity	Ratio of the area of a rectangle (formed with length and width as sides) to the area of the object
	Solidity	Ratio of the area of the object to the area of the convex hull of the object
	Convexity	Ratio of the perimeter of the convex outline of the object to the perimeter of the object

values of this parameter show that the grains of a rock are more oriented to a specific direction. From Table 2, it can be deduced that if grains of a rock were randomly oriented, its mean that orientation would be around 90. Therefore, the higher the deviation between computed orientation of a rock and 90 is, the more oriented grains towards a specific direction the rock has. According to Table 3, the R25 sample, which is a fine-grained andesite is the most oriented sample. Fig. 5 shows a photomicrograph of the R25 sample, grains orientation of the sample can be compared with those of R26 (Fig. 3), R15 (Fig. 4), R4 [Fig. 6a] and R11 [Fig. 6b] samples. Moreover, modal composition of the studied rocks is obtained from segmented photomicrographs using manual classification of grains presented in Table 1. It is worth mentioning that under cross-polarized light different minerals regarding the angle between their thin sections and optical axes might show similar optical characteristics in a specific direction and cannot be recognized just based on a single image (e.g. quartz from plagioclase showing no twinning nor alteration). In such cases, thin sections were checked using a microscope to ensure that minerals are correctly classified.

Based on basic size and shape descriptors, some rock fabric coefficients are computed for each studied rock. Moreover, some mineralogical indices, which are used in modal classification of igneous rocks (Jung and Brousse 1959), are computed using modal analysis of the rocks. The results are given in Table 3. The fabric coefficients and mineralogical indices are presented as follows:

Texture coefficient (TC) is a quantitative dimensionless coefficient which comprise grain shape parameters such as circularity, elongation, orientation of grains, and relative proportions of grains and matrix. The coefficient is calculated by the following formula that was suggested by Howarth and Rowlands (1987):

$$TC = AW \times \left[\left(\frac{N_0}{N_0 + N_1} \times \frac{1}{FF_0} \right) + \left(\frac{N_1}{N_0 + N_1} \right) \times AR_1 \times AF_1 \right]$$

(1)

where AW is the area weighting (grain packing density), N_0 is numbers of grains with aspect ratio (ratio of the maximum to the minimum Feret's diameter) less than 2.0, N_1 is numbers of grains with aspect ratio greater than 2.0, FF_0 is the arithmetic mean of form factor of all N_0 grains calculated using $\frac{4 \cdot \pi \cdot Area}{Perimeter^2}$, AR_1 is arithmetic mean of aspect ratio of N_1 grains, and AF_1 is angle factor orientation which were computed for all N_1 grains which is calculated using $\frac{1}{5} \sum_{i=1}^{9} \frac{1}{5}$ where N is the total number of elongated particles, Xi is the number of angular differences in each class and i is the weighing factor and class number.

Index of interlocking (g) is an arithmetic mean of proportion of rock grains perimeter which contacts neighboring grains quantified by square root of their respective area (Dreyer 1973). The increasing value of this parameter indicates a higher complexity of the grains' boundaries (Přikryl 2006). It is computed from the following formulas:

$$g = \frac{1}{n} \cdot \sum \frac{L_{pi}}{\sqrt{A_i}}$$

(2)

in which n is the number of grains considered, L_{pi} and A_i are the grain perimeter which contacts neighboring grains and grain area, respectively. It is notable that the index of interlocking of the R4 and the R11 samples are considered as zero, because these samples are two hyaline extrusive rocks, and their grains mostly do not contact with each other (Fig. 6).

Table 3 The petrographic features of the studied rocks

Rock code	Size descriptor					Shape descriptor							Fabric coefficient			Mineralogical index		
	Area (mm²)	Perimeter (mm)	Size (mm)	Min of Feret's (mm)	Max of Feret's (mm)	Elongation	Orientation (°)	Eccentricity	Compactness	Rectangularity	Solidity	Convexity	TC	g	t	IS	IF	IC
R1	0.07	1.59	0.27	0.26	0.44	1.70	1.40	4.48	0.36	1.04	0.71	0.78	2.26	6.33	0.064	33.73	36.36	17
R2	0.55	4.83	0.75	0.70	1.24	1.76	1.28	4.39	0.28	1.04	0.72	0.69	2.63	7.07	0.056	42.22	53.85	10
R3	0.47	4.34	0.67	0.64	1.08	1.68	1.69	3.91	0.30	1.02	0.71	0.70	3.23	6.92	0.051	36.05	61.82	14
R4	0.35	3.42	0.58	0.54	0.92	1.72	7.04	4.53	0.37	0.94	0.75	0.76	1.48	0.00	0.043	0.00	0.00	36
R5	0.51	4.55	0.67	0.63	1.14	1.81	10.44	4.27	0.32	1.04	0.71	0.73	2.64	6.80	0.047	34.41	44.26	7
R6	0.01	0.46	0.09	0.08	0.13	1.65	0.39	3.21	0.54	0.67	0.76	0.84	3.00	5.17	0.022	0.00	0.00	53
R7	0.54	4.68	0.66	0.63	1.11	1.77	3.70	4.92	0.28	1.06	0.70	0.70	3.05	7.22	0.039	41.11	58.49	10
R8	0.79	5.34	0.78	0.74	1.31	1.77	8.19	4.61	0.29	1.07	0.70	0.70	2.85	7.11	0.038	39.78	67.86	7
R9	0.59	4.88	0.71	0.66	1.23	1.86	10.50	5.23	0.29	1.07	0.70	0.71	2.49	7.11	0.040	43.16	74.07	5
R10	1.56	6.90	0.91	0.84	1.56	1.85	7.21	5.75	0.30	1.08	0.71	0.71	2.08	7.21	0.036	28.57	73.85	9
R11	0.23	2.81	0.47	0.44	0.78	1.78	2.85	4.52	0.37	0.97	0.73	0.77	1.70	0.00	0.055	23.08	16.66	22
R12	0.43	4.19	0.64	0.63	1.06	1.68	5.98	3.96	0.31	1.05	0.70	0.72	3.27	6.81	0.050	32.58	36.67	11
R13	0.18	2.84	0.43	0.41	0.72	1.77	8.99	5.35	0.29	1.12	0.70	0.72	2.71	7.12	0.088	18.42	25.81	24
R14	0.13	2.37	0.33	0.32	0.57	1.79	0.33	4.86	0.28	1.21	0.67	0.70	2.90	7.45	0.035	16.22	4.84	26
R15	0.57	5.35	0.74	0.72	1.33	1.86	9.97	6.39	0.26	1.19	0.68	0.69	2.55	7.54	0.052	1.52	1.54	34
R16	0.09	2.07	0.30	0.28	0.52	1.83	8.00	5.27	0.29	1.20	0.67	0.72	3.16	7.27	0.047	5.48	8.70	27
R17	1.05	6.68	0.97	0.92	1.62	1.77	12.21	4.67	0.28	1.06	0.71	0.68	2.89	7.31	0.057	30.43	54.69	8
R18	0.17	2.70	0.41	0.39	0.67	1.71	2.64	4.41	0.27	1.17	0.69	0.69	2.93	7.28	0.071	0.00	0.00	52
R19	0.16	2.83	0.40	0.39	0.69	1.78	10.53	5.25	0.26	1.20	0.68	0.69	3.03	7.57	0.065	0.00	0.00	64
R20	0.25	3.19	0.47	0.44	0.80	1.81	9.83	5.35	0.29	1.13	0.70	0.71	2.57	7.15	0.060	0.00	3.39	41
R21	0.29	3.84	0.53	0.50	0.92	1.83	2.54	5.13	0.25	1.19	0.67	0.67	2.95	7.73	0.049	0.00	4.92	39
R22	1.08	6.66	0.92	0.86	1.61	1.87	10.97	5.35	0.27	1.06	0.71	0.69	2.74	7.34	0.041	14.94	55.41	13
R23	1.16	7.60	0.98	0.94	1.69	1.80	7.64	4.58	0.24	1.14	0.69	0.65	2.80	7.80	0.063	7.69	52.38	9
R24	1.83	9.09	1.21	1.18	2.04	1.73	10.12	5.05	0.27	1.10	0.71	0.67	2.24	7.62	0.079	13.04	70.00	8
R25	0.02	0.93	0.13	0.12	0.24	1.93	19.29	5.49	0.26	1.16	0.67	0.69	2.35	7.54	0.083	3.80	9.21	21
R26	1.06	6.71	1.03	0.97	1.67	1.74	2.39	4.54	0.30	0.98	0.73	0.70	2.77	6.97	0.083	31.03	31.67	13
R27	1.20	6.33	0.99	0.91	1.61	1.77	1.08	4.78	0.31	0.99	0.74	0.72	2.63	6.77	0.046	34.94	16.67	17
R28	0.07	1.88	0.26	0.25	0.45	1.78	5.23	5.00	0.28	1.28	0.65	0.71	3.04	7.54	0.033	0.00	0.00	39

*TC: Texture coefficient; g: Index of interlocking; t: Index of grain size homogeneity; IS: Saturation Index; IF: Feldspathic Index; IC: Colouration Index
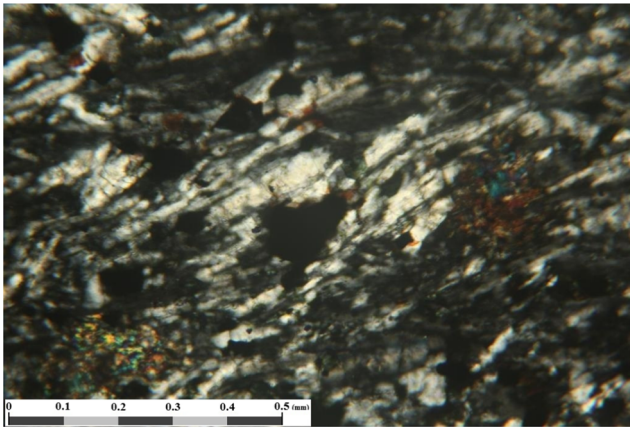
Fig. 5 Photomicrograph of R25 sample

Index of grain size homogeneity (t) is a fabric parameter describing grain size distribution in the material (Dreyer 1973):

$$t = \frac{A_{avg}}{\sqrt{\sum(A_i - A_{avg})^2}} \quad (3)$$

where A_{avg} is the average area of the grains and A_i is the area of individual grain.

Saturation Index (IS) is the ratio of the percentage of quartz (*Qtz*) to summed percentage of quartz and feldspars (*F*):

$$IS = \frac{Qtz\%}{(Qtz + Afs + Pl)\%} \times 100 \quad (4)$$

Feldspathic Index (IF) is the ratio of the percentage of alkali-feldspars (*Afs*) to summed percentage of alkali-feldspars and plagioclase (*Pl*):

$$IF = \frac{Afs\%}{(Afs + Pl)\%} \times 100 \quad (5)$$

Colouration Index (IC) is the sum of volume percentages of the colored, or dark, minerals contained in the rock:

$$IC = 100 - (Qtz + Afs + Pl)\% \quad (6)$$

It is notable that for the computation of mineralogical indices of hyaline rocks, percentage of mineral phases is considered as 100.
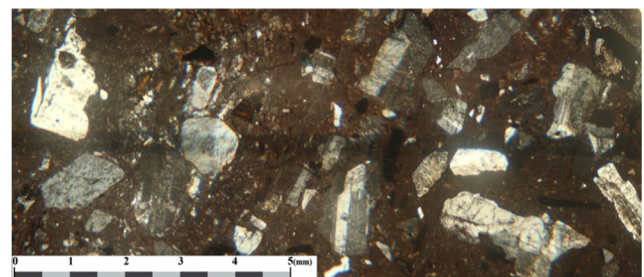
Engineering properties

In this study, each block sample was drilled or cut to obtain cylindrical cores or blocky specimens to inspect the physical, dynamic and mechanical properties. Various standard test procedures were carried out to determine engineering properties of the studied rocks. The basic physical properties of the rock samples including density and porosity were measured according to ISRM (1981). The P-wave velocity was determined using a Portable Ultrasonic Nondestructive Digital Indicating Tester (PUNDIT) according to ISRM (2007). Point load strength test was performed on blocky or core samples (axial test) according to ISRM (1985). Cerchar abrasivity test was conducted following the ISRM suggested method (Alber et al. 2014) by means of the modified Cerchar apparatus as reported by West (1989). The results are shown in Table 4.

Intact rock material strength is classified according to the magnitude of uniaxial compressive strength or point load index test results (Bieniawski 1989). The point load test is an attractive alternative to the UCS because it can provide similar data at a lower cost (Gurocak et al. 2012). Also, the point load strength index can be used to predict other strength parameters such as uniaxial tensile and compressive strengths (Broch and Franklin 1972; ISRM 1985; Kahraman 2001; Lashkaripour 2002; Palchik and Hatzor 2004; Heidari et al. 2012; Kohno and Maeda 2012; Li and Wong 2013).

Rock abrasivity has become one of the necessary parameters for mechanical excavation of rock in the tunneling industry (Hassanpour et al. 2011). The Cerchar abrasivity index (CAI) is a common method of predicting abrasiveness in excavation tools (Moradizadeh et al. 2016). The Cerchar abrasivity test has also been employed by Colorado School of Mines to predict the cutter life of the hard rock TBMs (Rostami et al. 1996). Some researchers have investigated the petrographic features affecting CAI (Suana and Peters
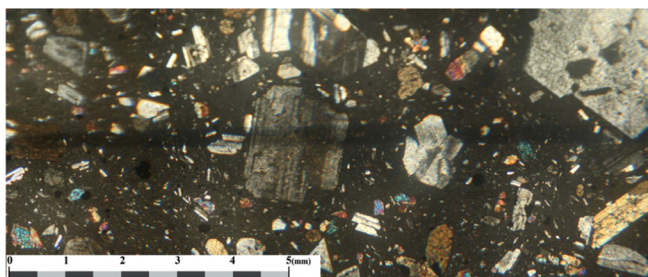
(a)

(b)

Fig. 6 Unified images from samples R4 (**a**) and R11 (**b**)

Table 4 Engineering properties of the studied rocks

Rock code	Dry density (gr/cm^3)	Porosity (%)	P-Wave velocity (m/s)	CAI (mm/10)	$I_{S(50)}$ (MPa)
R1	2.72	1.13	4841	4.3	6.14
R2	2.63	1.01	4451	4.0	6.72
R3	2.62	1.25	4301	4.1	5.63
R4	2.65	0.65	5715	3.2	9.78
R5	2.64	1.4	5406	3.3	7.77
R6	2.91	0.89	6193	3.3	14.64
R7	2.63	0.87	5109	4.1	7.72
R8	2.62	0.86	5064	4.5	7.65
R9	2.62	0.84	5195	4.6	8.69
R10	2.69	0.76	5136	3.8	5.49
R11	2.59	1.91	5351	2.7	10.24
R12	2.64	1.49	4115	3.2	7.78
R13	2.72	2.76	4394	3.9	8.36
R14	2.75	0.57	6156	2.9	12.29
R15	2.89	0.67	5422	3.0	11.93
R16	2.69	1.26	5825	3.1	8.69
R17	2.62	1.31	4555	4.5	6.91
R18	2.98	0.55	6182	2.6	11.41
R19	3.14	0.18	7239	2.8	12.29
R20	2.83	0.18	6365	2.9	11.08
R21	2.78	0.26	6342	2.9	10.87
R22	2.58	2.31	5246	3.6	7.00
R23	2.63	1.46	5135	3.4	8.19
R24	2.56	3.57	4531	3.1	5.59
R25	2.64	0.74	5783	2.9	10.49
R26	2.66	1.07	4277	3.8	7.27
R27	2.65	1.19	5367	4.4	6.07
R28	2.89	0.29	6491	3.0	10.68

1982; Lassnig et al. 2008; Rostami et al. 2014; Selman Er and Tugrul 2016). From these studies it is readily evident that both rock fabric and mineralogical characteristics have important effects on the abrasiveness potential of rocks.

Results and discussion

Correlations between the petrographical and the engineering properties

To control the effectiveness of the proposed semi-automatic petrographic analysis, firstly the Pearson's correlation coefficient (R) is employed:
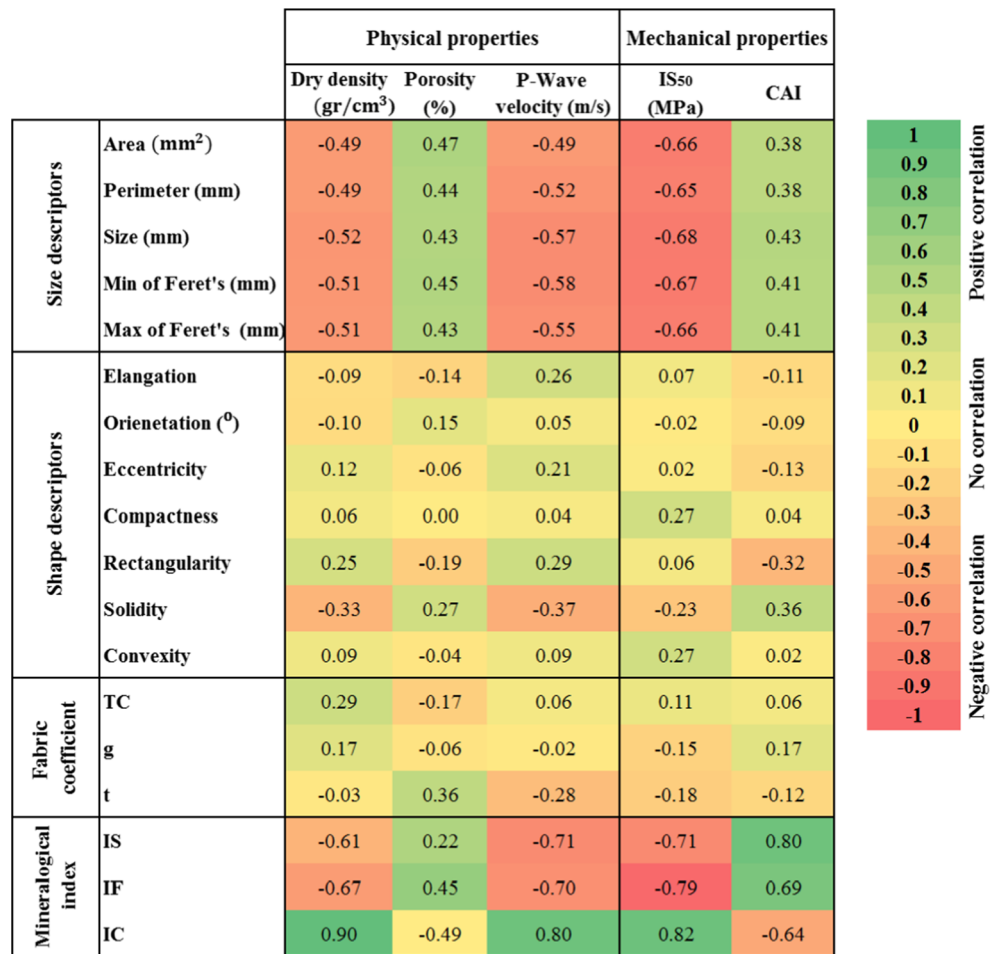
$$R_{xy} = \frac{\text{cov}(x, y)}{s_x s_y} \tag{7}$$

where to find the correlation between the variables by dividing the covariance by their standard deviations.

From the results, it is obvious that among evaluated petrographic features mineralogical composition, as well as size descriptors have more correlation with engineering properties of the igneous rocks (Fig. 7). From Fig. 7, no meaningful correlations between engineering properties and neither individual shape descriptors nor fabric coefficients can be established. Texture coefficient as an index can be considered as a significant and valid parameter to describe and classify different lithotypes (Howarth and Rowlands 1987; Ozturk and Nasuf 2013; Tandon and Gupta 2013), but as noted by Azzoni et al. (1996) and proved later by Přikryl (2006), and regarding the result of the present study, it is not reliable for accurately predicting mechanical properties of all lithologies. The failure of rock fabric coefficients including texture coefficient, index of interlocking, and index of grain size homogeneity is probably because these measures ignore the effect of both grain size and mineralogical composition of the studied rocks.

As shown in Fig. 7, it can be clearly seen that coarse-grained igneous rocks have lower strength, dry density and P-wave velocity generally. In different studies, it is reported

Fig. 7 Pearson's correlation coefficient between petrographical features and engineering properties of the studied rocks

		Physical properties			Mechanical properties	
		Dry density (gr/cm³)	Porosity (%)	P-Wave velocity (m/s)	IS50 (MPa)	CAI
Size descriptors	Area (mm²)	-0.49	0.47	-0.49	-0.66	0.38
	Perimeter (mm)	-0.49	0.44	-0.52	-0.65	0.38
	Size (mm)	-0.52	0.43	-0.57	-0.68	0.43
	Min of Feret's (mm)	-0.51	0.45	-0.58	-0.67	0.41
	Max of Feret's (mm)	-0.51	0.43	-0.55	-0.66	0.41
Shape descriptors	Elangation	-0.09	-0.14	0.26	0.07	-0.11
	Orienetation (°)	-0.10	0.15	0.05	-0.02	-0.09
	Eccentricity	0.12	-0.06	0.21	0.02	-0.13
	Compactness	0.06	0.00	0.04	0.27	0.04
	Rectangularity	0.25	-0.19	0.29	0.06	-0.32
	Solidity	-0.33	0.27	-0.37	-0.23	0.36
	Convexity	0.09	-0.04	0.09	0.27	0.02
Fabric coefficient	TC	0.29	-0.17	0.06	0.11	0.06
	g	0.17	-0.06	-0.02	-0.15	0.17
	t	-0.03	0.36	-0.28	-0.18	-0.12
Mineralogical index	IS	-0.61	0.22	-0.71	-0.71	0.80
	IF	-0.67	0.45	-0.70	-0.79	0.69
	IC	0.90	-0.49	0.80	0.82	-0.64

1	
0.9	Positive correlation
0.8	
0.7	
0.6	
0.5	
0.4	
0.3	
0.2	
0.1	
0	No correlation
-0.1	
-0.2	
-0.3	
-0.4	
-0.5	Negative correlation
-0.6	
-0.7	
-0.8	
-0.9	
-1	

that mean grain size of rock has an inverse relationship with strength properties of rocks (Onodera and Asoka Kumara 1980; Tugrul and Zarif 1999; Přikryl 2006). As mentioned by Přikryl (2006) an explanation of this phenomenon based on Griffith's theory is given by Brace (1961) who supposed the close connection between Griffith's crack length and maximum grain size diameter.

Since igneous rocks have a variety of different mineralogical compositions, in this study saturation index, feldspathic index and coloration index, which are used in French modal classification of igneous rocks, are employed to correlate with engineering properties. Such mineralogical indices could

efficiently incorporate mineral variations in igneous rocks. According to Fig. 7, there are some negative correlations between IS and index properties of the studied rocks including density, P-wave velocity and point load strength. There is also a good positive correlation between the IS and CAI, which shows the high abrasiveness potential of acidic igneous rocks. There are quite similar correlations between IF and engineering properties. In contrast, the IC decreases as the CAI increases. Also, direct relationships exist between IC, density, P-wave velocity and point load strength. As can be seen from Fig. 7, there are significant correlation between engineering properties and IC, with the exception of porosity which it is

Table 5 Correlations of the engineering properties of the studied rocks

R^2 / R	Dry density (gr/cm³)	Porosity (%)	P-Wave velocity (m/s)	$I_{S(50)}$ (MPa)	CAI (mm/10)
Dry density (gr/cm³)		0.31	0.54	0.52	0.24
Porosity (%)	−0.56		0.38	0.26	0.02
P-Wave velocity (m/s)	0.73	−0.61		0.59	0.37
$I_{S(50)}$ (MPa)	0.72	−0.51	0.77		0.44
CAI	−0.49	0.15	−0.61	−0.66	

expected. It is worth mentioning that this experimental study showed that plagioclase and ferromagnesian minerals except mica establish positive effects on engineering properties of the tested rocks, but quartz, alkali feldspars and mica minerals (biotite and muscovite) show negative effects on engineering properties of igneous rocks. In general, based on the results of laboratory tests and petrographic analysis of the studied un-weathered igneous rocks, it might be concluded that fine-grained and basic igneous rocks compared to the acidic and coarse-grained rocks possess higher engineering quality and lower abrasiveness potential.

Correlations of the engineering properties

There are numerous studies in the literature proposing empirical correlations between mechanical, physical and dynamical properties of various rock types (see e.g. Deere and Miller 1966; Palchik 1999; Kilic and Teymen 2008; Azimian 2017; Aligholi et al. 2017c). From the results of the present study there are direct relationships between density, P-wave velocity and point load strength index (Table 5). Also, there are negative correlations between CAI and previously mentioned engineering properties. In other words, basic rocks have higher strength and lower abrasiveness potential.

Table 5 confirm that studied engineering properties are more or less independent from each other, and reflecting a variety of different properties of the studied igneous rocks. Therefore, selected engineering properties are good options for evaluation of micropetrographic data in order to predict engineering properties of igneous intact rocks.

Multiple linear regression model

Most problems in mining and geology involve complex and interacting forces, which are impossible to isolate and study separately (Davis 1973). Engineering properties of rocks might be affected by multiple petrographic features such as mineralogy and modal composition, grain size, grain size homogeneity, grain shape, degree of interlocking, fractures and discontinuities, weathering and alterations; so, for a reliable and robust prediction of rock engineering properties, a reasonable combination of some petrographic features is required. Multiple regression analysis is a powerful modeling technique, which can help in the evaluation of the mechanical properties of rock (Cobanoglu and Celik 2008).

Ulusay et al. (1994) used multivariate regression models to investigate relationships between engineering properties and petrographic characteristics of some litharenite sandstones. Multivariate regression models are recently employed by some researchers for rock engineering properties prediction from simple methods (Karakus et al. 2005; Yilmaz and Yuksek 2009; Gurocak et al. 2012; Minaeian and Ahangari

Table 6 Summary of the multiple regression models and some statistical parameters on evaluation of validity of developed models

Dependent variable		Dry density (g/cm^3)	Porosity (%)	P-Wave velocity (m/s)	IS(50) (MPa)	CAI (mm/10)
Constant		5.3050	−17.195	−47,196	63.765	51.529
Regression coefficient of independent variables	Area (mm^2)	0.0023	2.1210	−570.54	−1.1841	−0.3663
	Perimeter (mm)	0.1199	−1.6088	1475.6	2.0366	−0.3242
	Size (mm)	0.6045	−54.543	3432.2	−56.205	39.644
	Min of Feret's (mm)	−3.0458	29.052	12,144	−13.938	−46.555
	Max of Feret's (mm)	0.9725	20.675	−14,269	32.589	4.2615
	Elangation	−0.7942	−3.0272	14,840	−3.4364	−13.304
	Orienetation (^{0})	0.0058	−0.0172	1.9559	0.1527	0.0425
	Eccentricity	−0.0031	−0.2177	−812.23	0.1301	0.7748
	Compactness	1.2809	−6.5062	−6843.7	112.56	14.429
	Rectangularity	0.1371	2.9303	5075.0	13.566	−2.4908
	Solidity	−3.0899	28.963	19,019	2.2468	−24.287
	Convexity	−0.1793	5.8506	16,961	−138.93	−18.682
	g	0.0037	−0.0252	38.415	−0.4606	0.0437
	t	1.3889	19.955	−15,176	5.2283	−0.1394
	IS	0.0072	−0.0195	8.4220	0.1444	0.0123
	IF	−0.0016	0.0035	−0.5043	−0.0841	0.0062
	IC	0.0115	−0.0322	58.903	0.0700	−0.0199
Performance index	R2	0.98	0.71	0.97	0.93	0.87
	RMSE	0.04	0.68	244	1.07	0.37
	p-Value	0.0000	0.2730	0.0000	0.0013	0.0151

2013; Aligholi et al. 2017a, c), and better results than simple regression analysis are reported.

In order to describe the relationships between multiple petrographic features and engineering properties of the tested rocks, multiple regression model with a 95% confidence level by considering linear functions were applied:

$$Y = \beta_0 + \beta_1 x_1 + \beta_2 x_2 + \cdots + \beta_n x_n \qquad (8)$$

where Y is the dependent variable, β_0 is a constant value, x_l to xn are the independent variables, and β_1 to β_n are partial regression coefficients for x_l to xn. The results of the regression analyses are given in Table 6. To check the validation of the statistical models, the measured engineering properties values are plotted versus the predicted values from these models (Fig. 8). It can be clearly seen that, with the exception of the porosity predictive model (Fig. 8d), points are distributed nearly uniformly around the diagonal lines, that proved the validity of proposed models.

As shown by Table 6, as it is expected only the statistical model developed to prediction of porosity from petrographic features fails to reject the null hypothesis at the default $\alpha =$
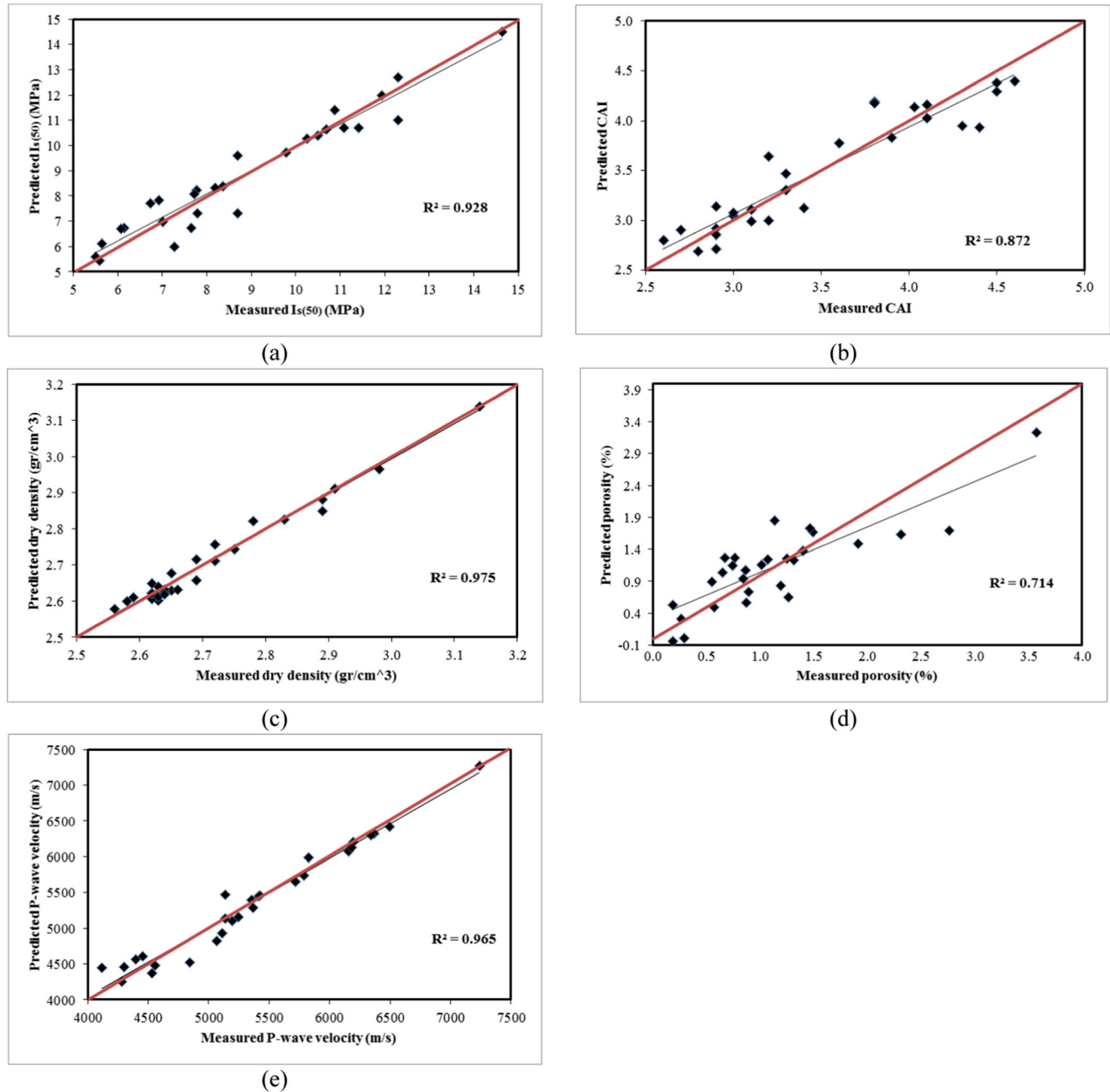
Fig. 8 Graphs of the predicted engineering properties from petrographical analysis versus the measured engineering properties: $I_{S(50)}$ (**a**), CAI (**b**), Dry density (**c**), Porosity (**d**), and P-wave velocity (**e**)

0.05 significance level, and other models are statistically significant. To control the performance of developed models, the root mean square errors (RMSE) was calculated for each model, from the following formulas:

$$RMSE = \sqrt{\frac{1}{N} \sum_{i=1}^{N} \left(y_i - y_i' \right)} \qquad (9)$$

where y and y′ are the measured and predicted values and N is the number of samples. If the R-squared (R^2) is 1 and RMSE is 0, the model proposed would be excellent.

Conclusion

This paper proposes a semi-automatic micropetrographic image analysis scheme, which is relatively simple and requires no sophisticated equipments for image acquisition. The proposed method is based on extraction and integration of seventeen petrographic features including size descriptors (1. Area; 2. Perimeter; 3. equivalent circular diameter; 4. minimum Feret's diameter; 5. maximum Feret's diameter), shape descriptors (6. elongation; 7. orientation; 8. eccentricity; 9. compactness; 10. rectangularity; 11. solidity; 12. convexity), rock fabric coefficients (13. index of interlocking; 14. index of grain size homogeneity) and mineralogical indices (15. saturation index; 16. feldspathic index; 17. colouration index), and is designed to allow rapid assessment of engineering properties of igneous rocks. The adopted methodology in this procedure involves: (1) generation of representative images using digital microscopy, (2) pre-processing and segmentation of images, (3) petrographic feature extraction, and (4) multivariate regression analysis for accurate prediction of engineering properties. The computer-aided procedure is examined for its performance and efficiency by using typical engineering properties such as density, porosity, P-wave velocity, strength and abrasivity of a wide range of Iranian igneous rocks.

This paper sheds further light on the relationships between petrographic features of igneous rocks and the engineering properties mentioned above. Based on the results of this study, the following conclusions may be reached:

1. The study revealed that the influence of mineralogical composition on engineering properties of igneous rocks appears to be more important than rock fabric characteristics.
2. Among rock fabric characteristics, size descriptors have significant influence on the engineering properties.
3. Generally, fine-grained and basic igneous rocks possess higher engineering quality and lower abrasiveness potential in comparison with the acidic and coarse-grained ones.
4. We found no meaningful correlation between the engineering properties and texture coefficients of the studied igneous rocks.
5. Multivariate regression analysis is an efficient method for the sake of petrographic analyses.
6. Our statistical models suggest that rock fabric features and mineralogical composition make fine complements for predicting the engineering properties of igneous rocks, and that both of them must be considered for a complete quantitative micropetrographic data analysis.
7. The results obtained from multiple regression models prove the efficiency and success of such models in predicting engineering properties. This shows that selected mineralogical and rock fabric features are significantly efficient in the engineering properties prediction of igneous rocks, and if a well-organized method is available, such features might be sufficient for an accurate prediction procedure, which in many cases can avoid time-consuming and tedious test methods.

Because of the petrographic variety and structural complexity, igneous rocks exhibit a wide range of engineering behaviors that may affect tunneling, mining, slope stability and their use as a construction material. This research, however, concludes that petrographic quantification using the proposed semi-automatic method is a reliable and inexpensive approach for analyzing the engineering properties of igneous rocks.

References

Akesson U, Stingh J, Lindqvist JE, Goransson M (2003) The influence of foliation on the fragility of granitic rocks, image analysis and quantitative microscopy. Eng Geol 68(3–4):275–288

Alber M, Yarali O, Dahl F, Bruland A, Kasling H, Michalakopoulos TN, Cardu M, Hagan P, Aydin H, Ozarslan A (2014) ISRM suggested method for determining the abrasivity of rock by the CERCHAR abrasivity test. Rock Mech Rock Eng 47:261–266

Aligholi S, Khajavi R, Razmara M (2015) Automated mineral identification algorithm using optical properties of crystals. Comput Geosci 85:175–183

Aligholi S, Lashkaripour GR, Ghafoori M, TrighAzali S (2017a) Evaluating the relationships between NTNU/SINTEF drillability indices with index properties and petrographic data of hard igneous rocks. Rock Mech Rock Eng 50(11):2929–2953

Aligholi S, Lashkaripour GR, Khajavi R, Razmara M (2017b) Automatic mineral identification using color tracking. Pattern Recogn 65:164–174

Aligholi S, Lashkaripour GR, Ghafoori M (2017c) Strength/brittleness classification of igneous intact rocks based on basic physical and dynamic properties. Rock Mech Rock Eng 50(1):45–65

Anon (1995) The description and classification of weathered rocks for engineering purposes, geological society engineering group working party report. Q J Eng Geol 28:207–242

Asmussen P, Conrad O, Günther A, Kirsch M, Riller U (2015) Semi-automatic segmentation of petrographic thin section images using a "seeded-region growing algorithm" with an application to characterize wheathered subarkose sandstone. Comput Geosci 83:89–99

Azimian A (2017) Application of statistical methods for predicting uniaxial compressive strength of limestone rocks using nondestructive tests. Acta Geotech 12:321–333

Azzoni A, Bilo F, Rondena E, Zaninetti A (1996) Assessment of texture coefficient for different rock types and correlation with uniaxial compressive strength and rock weathering. Rock Mech Rock Eng 29:36–46

Barraud J (2006) The use of watershed segmentation and GIS software for textural analysis of thin sections. J Volcanol Geotherm Res 154:17–33

Bell FG (1978) The physical and mechanical properties of the fell sandstones, Northumberland England. Eng Geol 12:1–29

Bieniawski ZT (1989) Engineering rock mass classifications. Wiley, New York

Brace WF (1961) Dependence of fracture strength of rocks on grain size. Proceedings of the 4th Symposium Rock Mechanics. University Park, Pennsylvania, pp 99–103

Broch EM, Franklin JA (1972) The point load strength test. Int J Rock Mech Min Sci Geomech Abstr 9:669–697

Brosch FJ, Schachner K, Blumel M, Fasching A, Fritz H (2000) Preliminary investigation results on fabrics and related physical properties of an anisotropic gneiss. J Struct Geol 22:1773–1787

Cobanoglu I, Celik SB (2008) Estimation of uniaxial compressive strength from point load strength, Schmidt hardness and P-wave velocity. Bull Eng Geol Environ 67:491–498

Davis JC (1973) Statistics and data analysis in geology. Wiley, New York

Deere DU, Miller RP (1966) Engineering classification and index properties for intact rocks. Tech Rep no. AFNL-TR-65-116, Air Force Weapons Laboratory, New Mexico

Dreyer W (1973) The Science of Rock Mechanics. Part I. The Strength Properties of Rocks, 2nd ed. Series on Rock and Soil Mechanics, vol. 1 (1971/73), No. 2. Trans Tech Publications, Clausthal

Er S, Tugrul A (2016) Estimation of Cerchar abrasivity index of granitic rocks in Turkey by geological properties using regression analysis. Bull Eng Geol Environ 75(3):1325–1339

Fahy MP, Guccione MJ (1979) Estimating strength of sandstone using petrographic thin section data. Bull Assoc Eng Geol 16:467–485

Filho IM, Spina TV, Falcao AX, Vidal AC (2013) Segmentation of sandstone thin section images with separation of touching grains using optimum path fores operators. Comput Geosci 57:146–157

Fueten F, Mason J (2007) An artificial neural net assisted approach to editing edges in petrographic images collected with the rotation polarizer stage. Comput Geosci 33:1176–1188

Goodchild JS, Fueten F (1998) Edge detection in petrographic images using the rotating polarizer stage. Comput Geosci 24:745–751

Gunsallus KL, Kulhawy FH (1984) A comparative evaluation of rock strength measures. Int J Rock Mech Min Sci Geomech Abstr 21:233–248

Gupta V, Sharma R (2012) Relationship between textural, petrophysical and mechanical properties of quartzites: a case study from northwestern Himalaya. Eng Geol 135–136:1–9

Gurocak Z, Solanki P, Alemdag S, Zaman MM (2012) New considerations for empirical estimation of tensile strength of rocks. Eng Geol 145–146:1–8

Hashemnejad A, Ghafoori M, TrighAzali S (2016) Utilizing water, mineralogy and sedimentary properties to predict LCPC abrasivity coefficient. Bull Eng Geol Environ 75(2):841–851

Hassanpour J, Rostami J, Zhao J (2011) A new hard rock TBM performance prediction model for project planning. Tunn Undergr Space Technol 26:595–603

Hatzor YH, Palchik V (1997) The influence of grain size and porosity on crack initiation stress and critical flaw length in dolomites. Int J Rock Mech Min Sci 34:805–816

Heidari M, Khanlari G, Torabi-Kaveh M, Kargarian S (2012) Predicting the uniaxial compressive and tensile strengths of gypsum rock by point load testing. Rock Mech Rock Eng 45(2):265–273

Heilbronner R (2000) Automatic grain boundary detection and grain size analysis using polarization micrographs or orientation images. J Struct Geol 22:969–981

Howarth DF, Rowlands JC (1987) Quantitative assessment of rock texture and correlation with drillability and strength properties. Rock Mech Rock Eng 20:57–85

Hugman RH, Friedman M (1979) Effects of texture and composition on mechanical behavior of experimentally deformed carbonate rocks. Am Assoc Pet Geol Bull 63(9):1478–1489

ISRM. In: Brown ET (Ed.) (1981) Rock characterization testing and monitoring — ISRM suggested methods. Pergamon, New York

ISRM (1985) Suggested methods for determining point load strength. Int J Rock Mech Min Sci Geomech Abst 22(2):51–60

ISRM (2007) The complete ISRM suggested methods for rock characterization, testing and monitoring: 1974–2006. In: Ulusay R, Hudson JA (eds.). Suggested methods prepared by the commission on testing methods, International Society for Rock Mechanics, Compilation Arranged by the ISRM Turkish National Group, Ankara

Izadi H, Sadri J, Mehran NA (2015) A new intelligent method for minerals segmentation in thin sections based on a novel incremental color clustering. Comput Geosci 81:38–52

Jeng FS, Weng MC, Lin ML, Huang TH (2004) Influence of petrographic parameters on geotechnical properties of tertiary sandstone from Taiwan. Eng Geol 73:71–91

Jin X (2012) Segmentation-based image processing system. U.S. Patent 8,260,048; filed Nov. 14, 2007, and issued Sept. 4, 2012

Jung J, Brousse R (1959) Classification modale des roches éruptive.s: roches éruptive.s utilizant les données fournies par le compteur de points. Paris: Masson & Cie

Kahraman S (2001) Evaluation of simple method for assessing the uniaxial compressive strength of rock. Int J Rock Mech Min Sci 38:981–994

Karakus M, Kumral M, Kilic O (2005) Predicting elastic properties of intact rocks from index tests using multiple regression modeling. Int J Rock Mech Min Sci 42:323–330

Kilic A, Teymen A (2008) Determination of mechanical properties of rocks using simple methods. Bull Eng Geol Environ 67(2):237–244

Kohno M, Maeda H (2012) Relationship between point load strength index and uniaxial compressive strength of hydrothermally altered soft rocks. Int J Rock Mech Min Sci 50:147–157

Lashkaripour GR (2002) Predicting mechanical properties of mudrock from index parameters. Bull Eng Geol Environ 61(1):73–77

Lassnig K, Latal C, Klima K (2008) Impact of grain size on the cerchar abrasiveness test. Geomech Tunn 1:71–76

Li D, Wong LNY (2013) Point load test on meta-sedimentary rocks and correlation to UCS and BTS. Rock Mech Rock Eng 46:889–896

Marschallinger R, Hofmann P (2010) The application of object based image analysis to petrographic micrographs. Microsc Sci Technol Appl Educ 4:1526–1532

Middleton A, Freestone IC, Leese MN (1985) Textural analysis of ceramic thin sections: evaluation of grain sampling procedures. Archaeom 27(1):64–74

Minaeian B, Ahangari K (2013) Estimation of uniaxial compressive strength based on P-wave and Schmidt hammer rebound using statistical method. Arab J Geosci 6:1925–1931

Moradizadeh M, Cheshomi A, Ghafoori M, TrighAzali S (2016) Correlation of equivalent quartz content, slake durability index and Is_{50} with Cerchar abrasiveness index for different types of rock. Int J Rock Mech Min Sci 86:42–47

Obara B (2007) A new algorithm using image color system transformation for rock grain segmentation. Mineral Petrol 91:271–285

Olsson WA (1974) Grain size dependence of yield stress in marble. J Geophys Res 79(32):4859–4861

Onodera TF, Asoka Kumara HM (1980) Relation between texture and mechanical properties of crystalline rocks. Bull Assoc Eng Geol 22:173–177

Ozturk CA, Nasuf E (2013) Strength classification of rock material based on textural properties. Tunn Undergr Space Technol 37:45–54

Palchik V (1999) Influence of porosity and elastic modulus on uniaxial compressive strength in soft brittle porous sandstones. Rock Mech Rock Eng 32:303–309

Palchik V, Hatzor YH (2004) The influence of porosity on tensile and compressive strength of porous chalks. Rock Mech Rock Eng 37(4):331–341

Pappalardo G, Punturo R, Mineo S, Ortolano G, Castelli F (2016) Engineering geological and petrographic characterization of Migmatites belonging to the Calabria-Peloritani Orogen (southern Italy). Rock Mech Rock Eng 49(4):1143–1160

Přikryl R (2001) Some microstructural aspects of strength variation in rocks. Int J Rock Mech Min Sci 38(5):671–682

Přikryl R (2006) Assessment of rock geomechanical quality by quantitative rock fabric coefficients: limitations and possible source of misinterpretations. Eng Geol 87:149–162

Raisanen M (2004) Relationship between texture and mechanical properties of hybrid rocks from the Jaala-litti complex, southeastern Finland. Eng Geol 74:197–211

Reedy CL (2006) Review of digital image analysis of petrographic thin sections in conservation research. J Am Inst Conserv 45(2):127–146

Robinson DJ, Redding NJ, Crisp DJ (2002) Implementation of a fast algorithm for segmenting SAR imagery. Aust.: Sci. Tech. Rep. Defense Sci. Technol. Organiz

Ross BJ, Fueten F, Yashkir DY (2001) Automatic mineral identification using genetic programming. Mach Vis Appl 13:61–69

Rostami J, Ozdemir L, Nilson B (1996) Comparison between CSM and NTH hard rock TBM performance prediction models. In: Proceedings of Institute of Shaft Drilling Technology Annual Technical Conference, Las Vegas, Nevada, p 11

Rostami J, Ghasemi A, Gharahbagh E, Dogruoz C, Dahl F (2014) Study of dominant factors affecting Cerchar abrasivity index. Rock Mech Rock Eng 47(5):1905–1919

Streckeisen A (1976) To each plutonic rock its proper name. Earth Sci Rev 12:12–33

Suana M, Peters TJ (1982) The CERCHAR abrasivity index and its relation to rock mineralogy and petrography. Rock Mech 15(1):1–7

Tandon SR, Gupta V (2013) The control of mineral constituents and textural characteristics on the petrophysical & mechanical (PM) properties of different rocks of the Himalaya. Eng Geol 153:125–143

Thompson S, Fueten F, Bockus D (2001) Mineral identification using artificial neural networks and the rotating polarizer stage. Comput Geosci 27:1081–1089

Tugrul A, Zarif IH (1999) Correlation of mineralogical and textural characteristics with engineering properties of selected granitic rocks from Turkey. Eng Geol 51:303–317

Ulusay R, Tureli K, Ider MH (1994) Prediction of engineering properties of a selected litharenite sandstone from its petrographic characteristics using correlation and multivariate statistical techniques. Eng Geol 38(1–2):135–157

Vincent L (1993) Morphological grayscale reconstruction in image analysis: applications and efficient algorithms. IEEE Trans Image Process 2(2):176–201

Vincent L, Soille P (1991) Watershed in digital spaces: an efficient algorithm based on immersion simulations. IEEE Trans Pattern Anal Mach Intell 13(6):583–598

West G (1989) Rock abrasiveness testing for tunnelling. Int J Rock Mech Min Sci 26:151–160

Yilmaz I, Yuksek G (2009) Prediction of the strength and elasticity modulus of gypsum using multiple regression, ANN, and ANFIS models. Int J Rock Mech Min Sci 46(4):803–810

Yilmaz NG, Goktan RM, Kibici Y (2011) Relation between some quantitative petrographic characteristics and mechanical strength properties of granitic building stones. Int J Rock Mech Min Sci 48(3):506–513

Zhou Y, Starkey J, Mansinha L (2004) Segmentation of petrographic images by integrating edge detection and region growing. Comput Geosci 30:817–831

Zorlu K, Gokceoglu C, Ocakoglu F, Nefeslioglu HA, Acikalin S (2008) Prediction of uniaxial compressive strength of sandstone using petrography-based models. Eng Geol 96:141–158